

Exit versus escape a basin of attraction in noisy dynamical systems

Lou Zonca^{‡*} and David Holcman[†]

October 30, 2021

Abstract

We study a class of two-dimensional dynamical systems perturbed by small noise that exhibits a peculiar shift of the maximum associated to the probability density function from the point attractor. Using WKB approximation and numerical simulations, we examine the density of point inside the attractor and we found an algebraically relation for the distance between the maximum and the attractor with respect to the noise amplitude σ . For such systems, we further report that exiting from the basin of attraction is not sufficient to characterize the escape. Indeed, trajectories after crossing the boundary can return several times inside before eventually escaping far away. Finally, we apply the present results to study the distribution of the interburst durations in time series generated by mean-field model of excitatory neuronal networks.

Keywords: Stochastic dynamical systems, Asymptotic analysis, WKB, Escape from an attractor, Neuronal networks

1 Introduction

Noisy nonlinear dynamical systems exhibit peculiar behavior compared to deterministic ones: noise can lead to escape from a basin of attraction, dynamics can present large fluctuations away from the stable attractors [1–3] that can even induce switching in multi-stable systems. Noise can also enhance the response to periodic external stimuli, a phenomenon known as stochastic resonance [4]. For example, in the case of interaction between noise and a dynamics presenting a Hopf bifurcation, oscillations that would disappear in the deterministic case can be maintained [5]. Finally, noise can induce a shift in bifurcation values [6] or can stabilize an unstable equilibrium [7–9].

*Sorbonne University, Pierre et Marie Curie Campus, 5 place Jussieu 75005 Paris, France

†Group of Computational Biology and Applied Mathematics, Institut de Biologie de l'École Normale Supérieure, 46 rue d'Ulm 75005 Paris, France.

In the context of modeling biological neuronal networks, noise also plays a critical role for understanding collective rhythms or large synchronization. Mean-field models are used to reduce the complexity of large neuronal ensembles but still capture averaged behaviors using a projection to low dimensional dynamical systems [10]. Such models are used to study several behaviors such as bursting activity, synchronization and oscillation in excitatory neuronal networks [11–15]. However, in such models interburst duration was not much studied although it has recently been shown to contribute to the overall neuronal networks dynamics [16] and can even influence the bursting activity.

Studying the escape rate from a basin of attraction for a noisy dynamical system usually consists in collecting trajectories that terminate when they hit for the first time the boundary of the basin of attraction, which occurs with probability one [17, 18]. The escape rate and the distribution of exit points can be computed in the small noise limit using WKB approximation. Another interesting property is that the exit point distribution peaks at a distance $O(\sqrt{\sigma})$ from the saddle-point (where σ is the noise amplitude) [19, 20]. Metrics relation can also play a role in shaping the dynamics so that when a focus attractor falls into the boundary layer of the boundary, escaping trajectories exhibit periodic oscillations leading to an escape time distribution which is not exponential, because several eigenvalues are necessary to describe the distribution [21–26]. In the case of periodically-driven systems the escape rate is scaled by the field’s intensity [27, 28]. In all these examples, escape ends when a trajectory hits the separatrix for the first time which will not be the case for the systems we wish to study here. We consider here a class of dynamical systems perturbed by a white noise of small amplitude for which trajectories exiting the basin of attraction can reenter multiple times before eventually escaping to infinity. This effect requires to clarify the difference between exiting versus escaping that we explain below.

The manuscript is organized as follows: in the first part, we describe a generic two-dimensional dynamical system, containing an attractor and one saddle-point. We study a stochastic perturbation and show that the maximum of the probability density function of trajectories before escape is not centered at the attractor, but at a shifted location that depends on the noise amplitude σ . In the second part, we focus on the escape from the basin of attraction. We report, using numerical simulations, that after exiting, trajectories can return inside the basin of attraction multiple times before eventually escaping to infinity. We decompose the escape time on the contribution of each excursion outside the basin of attraction and show that the total escape time is increased by a factor between 2 and 3 compared to the first exit time. Finally, in the third part, we discuss these results in the context of a model describing bursting in excitatory neuronal networks [10, 15] thus providing a possible explanation for the distribution of long interburst intervals observed in experimental data [16].

2 Perturbation by Gaussian white noise induces a shift in the attractor's position in a 2D dynamical system

We consider the two-dimensional stochastic dynamical system

$$\begin{aligned} \dot{h} &= -\alpha h + x^2 + \sigma \dot{\omega} \\ \dot{x} &= \begin{cases} h - \gamma x & \text{for } h \geq 0 \\ -\gamma x & \text{for } h \leq 0, \end{cases} \end{aligned} \quad (1)$$

where $\alpha \in]0, 1]$, $\gamma \in]0, \alpha[$, $\dot{\omega}$ is a Gaussian white noise and σ its amplitude. This system has two critical points, $A = (0, 0)$ (fig. 1A yellow star) and $S = (\gamma^2\alpha, \gamma\alpha)$ (fig. 1A cyan star). The Jacobian of the system at point A can be computed either for $h \geq 0$ or for $h \leq 0$ and in both cases

$$J_A = \begin{pmatrix} -\alpha & 0 \\ 1 & -\gamma \end{pmatrix}. \quad (2)$$

A is an attractor with real eigenvalues $\lambda_1 = -\alpha$ and $\lambda_2 = -\gamma$ (its stable manifolds are shown in fig. 1A, dotted black lines). At point S , the first coordinate $h_S = \gamma^2\alpha > 0$ and thus the Jacobian is

$$J_S = \begin{pmatrix} -\alpha & 2\alpha\gamma \\ 1 & -\gamma \end{pmatrix}. \quad (3)$$

Its eigenvalues are both real, $\lambda_{\pm} = -\frac{1}{2} \left(-(\alpha + \gamma) \pm \sqrt{(\alpha + \gamma)^2 + 4\alpha\gamma} \right)$ thus S is a saddle point (with $\alpha = 1$ and $\gamma = 0.6$ we have $\lambda_+ \approx 0.314$ and $\lambda_- \approx -1.914$). The separatrix that delimits the basin of attraction of A is the stable manifold of S (fig. 1A solid black curve), the unstable manifold of which defines the escaping direction (fig. 1A yellow curve). It is located between the x (respectively h) nullcline $\Phi = \{(x, h) | h = \gamma x\}$, 1A red (respectively $\tilde{\Phi} = \{(x, h) | h = x^2/\alpha\}$, purple).

Using numerical simulations, we observe that trajectories are not centered around the deterministic attractor A (fig. 1B, green trajectory). We observe that the empirical distribution peaks at a point A_{σ} shifted towards the right of the deterministic attractor A (fig. 1B, green star).

2.1 Numerical study of the position of the shifted attractor A_{σ}

To better estimate the shift induced by noise in the attractor's position, we ran simulations of the stochastic model (1) (fig. 1B $\sigma = 0.09$, where trajectories are simulated for 500s). We observed that the trajectories loop around the x -nullcline Φ (red line). To characterize the shift in the distribution we study the distribution $\rho_{P_0} = P(\mathbf{s}(t) \in \Phi | \mathbf{s}(0) = A)$ of points P_0 where a stochastic trajectory starting at A hits Φ for the first time (fig. 1C, red). We generated the distribution ρ_{P_0} by simulating 150 trajectories (fig. 1D, red) and we found that this distribution is peaked at P_0 close to A . To further understand the

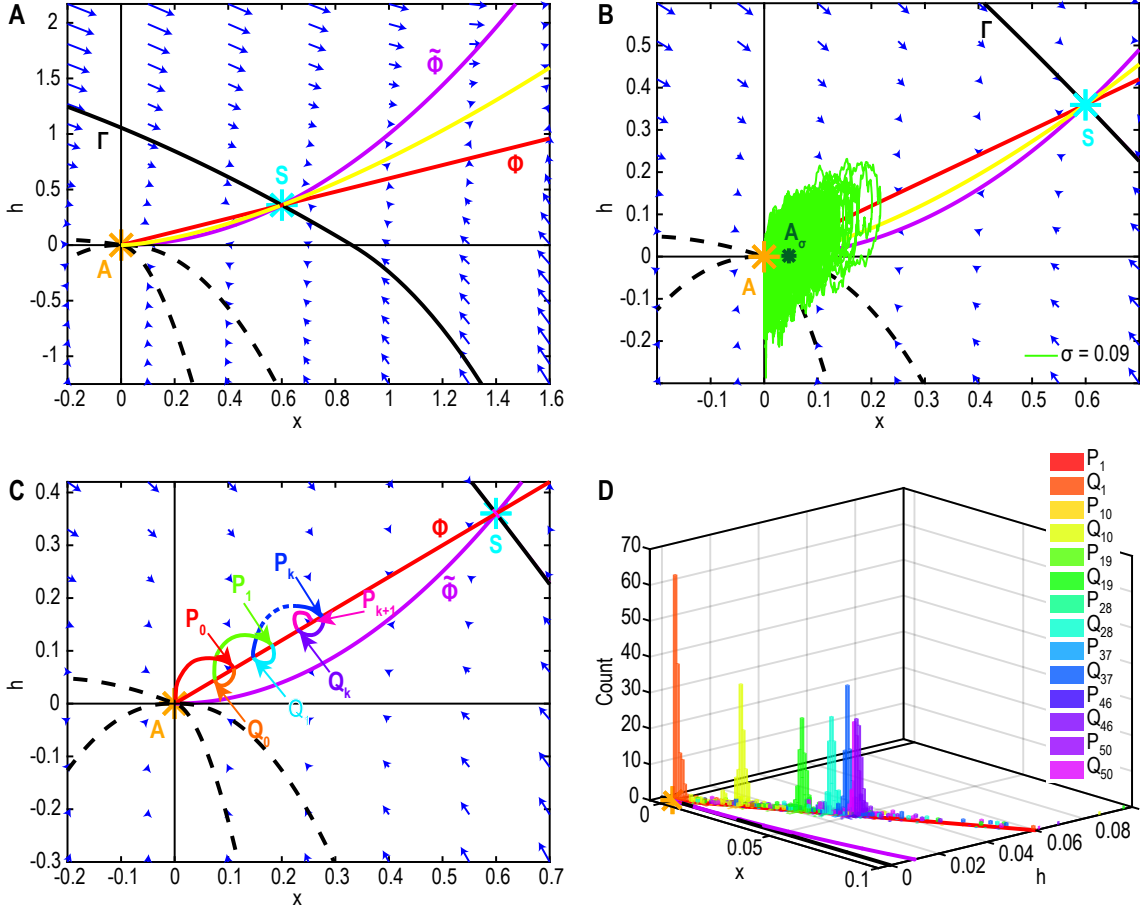


Figure 1: **Emergence of a shift in the attractor's position for the noisy dynamical system (1).** **A.** 2D phase-space of system (1), the deterministic basin of attraction of A (yellow) is delimited by the stable manifold (solid black) of the saddle-point S (cyan). The dashed lines indicate the stable manifolds of A . **B.** Stochastic trajectory ($\sigma = 0.09$, green) with its center of mass A_σ shifted towards the right ($x_{A_\sigma} \approx 0.05$). **C.** Schematic of successive intersection points P_k and Q_k of trajectories with Φ (red line). **D.** Distributions ρ_{P_k} and ρ_{Q_k} (500 runs, $\sigma = 0.09$) for $1 \leq k \leq 50$. The peak of the converging distributions $\rho_{P_{46}}$ to $\rho_{P_{50}}$ (purple) indicates the x -coordinate of the shifted attractor A_σ ($x_{A_\sigma} \approx 0.05$).

dynamics we investigated the distribution $\rho_{Q_0} = P(\mathbf{s}(t) \in \Phi | \mathbf{s}(0) = P_0)$ of points Q_0 where a trajectory starting at P_0 hits Φ for the first time (fig. 1C, orange). This distribution is also very peaked and located nearby ρ_{P_0} (fig. 1D, orange). We then iterated this process to obtain the successive distributions $\rho_{P_k} = P(\mathbf{s}(t) \in \Phi | \mathbf{s}(0) = P_k)$, where P_k are the points where a trajectory starting initially at Q_{k-1} hits Φ . Similarly, we define the distributions $\rho_{Q_k} = P(\mathbf{s}(t) \in \Phi | \mathbf{s}(0) = P_k)$ of the points where a trajectory starting at the peak of ρ_{P_k} hits Φ for the first time (fig. 1D). Interestingly, we observed that the distributions are peaked and progress along Φ towards the separatrix Γ . However, after a few iterations, the successive distributions ρ_{P_k} and ρ_{Q_k} , tend to accumulate and stop progressing, showing the position (along the x-coordinate) of the shifted equilibrium (fig. 1D, pink and purple distributions).

2.2 Computing the steady-state distribution and the distance of its maximum to the attractor A

2.2.1 Probability density function of system (1)

In this subsection we study the probability density function (pdf) of the system (1) for trajectories that stay inside the basin of attraction of A . We first generated 300s simulations for three values of the noise amplitude $\sigma = 0.03$ (pink), 0.09 (blue) and 0.12 green (fig. 2A) showing that the pseudo-distributions for points that do not escape the basin of attraction are peaked at A_σ shifted to the right of A . We shall now compute this pdf using WKB approximation [19]. The stochastic process is

$$d\mathbf{s} = \mathbf{B}(\mathbf{s})dt + \sqrt{\boldsymbol{\sigma}}dW, \quad (4)$$

where

$$\mathbf{B}(\mathbf{s}) = \begin{pmatrix} b_1(\mathbf{s}) = -\alpha h + x^2 \\ b_2(\mathbf{s}) = \begin{cases} h - \gamma x & \text{for } h \geq 0 \\ -\gamma x & \text{for } h \leq 0 \end{cases} \end{pmatrix}, \quad (5)$$

and

$$\sqrt{\boldsymbol{\sigma}} = \begin{pmatrix} \sqrt{\sigma} & 0 \\ 0 & 0 \end{pmatrix}. \quad (6)$$

The steady-state pdf $p(\mathbf{s})$ satisfies the stationary Fokker-Planck equation (FPE)

$$-(\nabla \cdot \mathbf{B})p - \mathbf{B} \cdot \nabla p + \frac{\sigma}{2} \frac{\partial^2 p}{\partial h^2} = \delta_A, \quad (7)$$

where δ_A is the δ -Dirac function at point A . We note that due to the discontinuity of the field at $h = 0$ we compute $\nabla \cdot \mathbf{B}$ on the two half spaces ($h \geq 0$) and ($h \leq 0$) separately. In small noise limit $\sigma \rightarrow 0$, the WKB solution has the form

$$p(\mathbf{s}) = K_\sigma(\mathbf{s}) e^{-\frac{\psi(\mathbf{s})}{\sigma}}, \quad (8)$$

where K_σ is a regular function that admits an expansion

$$K_\sigma(\mathbf{s}) = \sum_{i=0}^{\infty} K_i(\mathbf{s})\sigma^i. \quad (9)$$

The eikonal equation is obtained by injecting (8) in (7) and by keeping only the higher order terms in σ (ie σ^{-1})

$$\mathbf{B} \cdot \nabla\psi + \frac{1}{2} \left(\frac{\partial\psi}{\partial h} \right)^2 = 0 \quad (10)$$

and the transport equation is obtained with the terms of order 1

$$\mathbf{B} \cdot \nabla K_0 + \frac{\partial\psi}{\partial h} \frac{\partial K_0}{\partial h} = - \left(\nabla \cdot \mathbf{B} + \frac{1}{2} \frac{\partial^2\psi}{\partial h^2} \right) K_0. \quad (11)$$

We use the method of characteristics to solve (10). Using the previous notations and $q = (q_1, q_2) = \nabla\psi$, (10) becomes

$$F(\mathbf{s}, q, \psi) = \mathbf{B} \cdot q + \frac{1}{2}q_1^2 = 0 \quad (12)$$

the characteristics are given by

$$\begin{aligned} \frac{dh}{dt} &= b_1(\mathbf{s}) + q_1 \\ \frac{dx}{dt} &= b_2(\mathbf{s}) \\ \frac{dq_1}{dt} &= -F_h = -\frac{\partial b_1}{\partial h}q_1 - \frac{\partial b_2}{\partial h}q_2 \\ \frac{dq_2}{dt} &= -F_x = -\frac{\partial b_1}{\partial x}q_1 - \frac{\partial b_2}{\partial x}q_2 \\ \frac{d\psi}{dt} &= \frac{1}{2}q_1^2. \end{aligned} \quad (13)$$

To define the initial condition, we choose a neighborhood V_A of A (positioned at the origin), where ψ has a quadratic approximation

$$\psi(\mathbf{s}) \approx \frac{1}{2}\mathbf{s}^T R\mathbf{s} + o(|s|^2) \text{ for } \mathbf{s} \in V_A, \quad (14)$$

where R is a symmetric positive definite matrix defined by the matrix equation at A

$$(J_A\mathbf{s})^T \cdot \nabla\psi + \frac{1}{2}q_1^2 = 0, \quad (15)$$

where J_A is the Jacobian matrix at point A defined by relation (2). We obtain

$$\psi(\mathbf{s}) \approx \frac{1}{2} \mathbf{s}^T \begin{pmatrix} 2\alpha & 2\gamma \\ 2\gamma & 2\gamma \end{pmatrix} \mathbf{s}. \quad (16)$$

The ψ contours are the ellipsoids given by

$$\alpha h^2 + 2\gamma xh + \gamma x^2 = \epsilon, \quad (17)$$

for small $\epsilon > 0$. To conclude, we choose for the initial conditions one of the small ellipsoids given by (17) by fixing later on the value of ϵ .

2.2.2 Solution in the subspace $h \leq 0$

A direct integration of system (13) gives for $t \geq 0$

$$\begin{aligned} h(t) &= \left(h_0 - \frac{x_0^2}{\alpha - 2\gamma} - \frac{q_{1,0}}{2\alpha} \right) e^{-\alpha t} + \frac{x_0^2}{\alpha - 2\gamma} e^{-2\gamma t} + \frac{q_{1,0}}{2\alpha} e^{\alpha t} \\ x(t) &= x_0 e^{-\gamma t} \\ q_1(t) &= q_{1,0} e^{\alpha t} \\ q_2(t) &= \left(q_{2,0} - \frac{2x_0 q_{1,0}}{\alpha - 2\gamma} \right) e^{\gamma t} - \frac{2x_0 q_{1,0}}{\alpha - 2\gamma} e^{(-\gamma + \alpha)t} \\ \psi(t) &= \frac{q_{1,0}^2}{4\alpha} e^{2\alpha t}, \end{aligned} \quad (18)$$

where the initial conditions are $h(0) = h_0$, $x(0) = x_0$, $q_1(0) = q_{1,0}$ and $q_2(0) = q_{2,0}$. Substituting the expression of x and q_1 in h , we obtain

$$\psi(h, x) = \alpha \left(h - \left(h_0 - \frac{x_0^2}{\alpha - 2\gamma} - \frac{q_{1,0}}{2\alpha} \right) \left(\frac{x}{x_0} \right)^{\frac{\alpha}{\gamma}} - \frac{x^2}{\alpha - 2\gamma} \right)^2. \quad (19)$$

We solve the transport equation (11) along the characteristics (18). Using (1) and (19), we obtain

$$\frac{dK_0(\mathbf{s}(t))}{dt} = \gamma K_0(\mathbf{s}(t)) \quad (20)$$

yielding

$$K_0(\mathbf{s}(t)) = C e^{\gamma t}. \quad (21)$$

For $\alpha > \gamma$, and choosing $\mathbf{s}(t) \in V_A$

$$\tilde{\mathbf{s}}(t) \approx \int_0^t x_0 e^{-\gamma u} du \approx -x_0 \frac{e^{-\gamma t} - 1}{\gamma}. \quad (22)$$

Thus

$$K_0 \sim \frac{x_0}{x_0 + \gamma \mathbf{s} \cdot \mathbf{e}_2} = \frac{x_0}{x_0 + \gamma x}, \quad (23)$$

where $\mathbf{e}_2 = (0, 1)^T$ is the eigenvector associated to the eigenvalue $\lambda_2 = -\gamma$. Finally,

$$p(\mathbf{s}) \sim \frac{x_0}{x_0 + \gamma x} e^{-\frac{\psi(\mathbf{s})}{\sigma}}. \quad (24)$$

2.2.3 Solution in the subspace $\mathbf{h} \geq 0$

In this case, we cannot integrate system (13) analytically, however, close to A , $x \ll 1$ and since ψ is a smooth function, we neglect the quadratic terms in system (13) yielding

$$\begin{aligned} \frac{dh}{dt} &\approx -\alpha h + q_1 \\ \frac{dx}{dt} &= -\gamma x + h \\ \frac{dq_1}{dt} &= \alpha q_1 - q_2 \\ \frac{dq_2}{dt} &\approx -F_x = \gamma q_2 \\ \frac{d\psi}{dt} &= \frac{1}{2} q_1^2. \end{aligned} \quad (25)$$

Integration of system (25) gives, for $t \geq 0$

$$\begin{aligned} h(t) &= H_0 e^{-\alpha t} + \frac{Q_0}{2\alpha} e^{\alpha t} - \frac{q_{2,0}}{\gamma^2 - \alpha^2} e^{\gamma t} \\ x(t) &= X_0 e^{-\gamma t} + \frac{H_0}{\gamma - \alpha} e^{-\alpha t} + \frac{Q_0}{2\alpha(\gamma + \alpha)} e^{\alpha t} - \frac{q_{2,0}}{2\gamma(\gamma^2 - \alpha^2)} e^{\gamma t} \\ q_1(t) &= Q_0 e^{\alpha t} - \frac{q_{2,0}}{\gamma - \alpha} e^{\gamma t} \\ q_2(t) &= q_{2,0} e^{\gamma t} \\ \psi(t) &= \frac{Q_0^2}{4\alpha} e^{2\alpha t} + \frac{q_{2,0}^2}{4\gamma(\gamma - \alpha)^2} e^{2\gamma t} - \frac{Q_0 q_{2,0}}{\gamma^2 - \alpha^2} e^{(\gamma + \alpha)t}, \end{aligned} \quad (26)$$

where

$$\begin{aligned}
Q_0 &= q_{1,0} + \frac{q_{2,0}}{\gamma - \alpha} \\
H_0 &= h_0 - \frac{Q_0}{2\alpha} + \frac{q_{2,0}}{\gamma^2 - \alpha^2} \\
X_0 &= x_0 - \frac{H_0}{\gamma - \alpha} - \frac{Q_0}{2\alpha(\gamma + \alpha)} + \frac{q_{2,0}}{2\gamma(\gamma^2 - \alpha^2)}
\end{aligned} \tag{27}$$

and the initial conditions are $h(0) = h_0$, $x(0) = x_0$, $q_1(0) = q_{1,0}$ and $q_2(0) = q_{2,0}$. To derive the eikonal solution, we eliminate the time and start with the relation

$$q_2 \approx 2\gamma(h + x), \tag{28}$$

which is obtained from (16). Substituting (28) in h , we obtain near the attractor A

$$\psi(h, x) \approx \frac{Q_0^2}{4\alpha} \left(\frac{2\gamma(h+x)}{q_{2,0}} \right)^{\frac{2\alpha}{\gamma}} + \frac{\gamma(h+x)^2}{(\gamma-\alpha)^2} + \frac{Q_0 q_{2,0}}{\gamma^2 - \alpha^2} \left(\frac{2\gamma(h+x)}{q_{2,0}} \right)^{\frac{\alpha+\gamma}{\gamma}}. \tag{29}$$

Furthermore, we solve the transport equation (11) along the characteristics (26). We differentiate twice (29) with respect to h , we obtain $\frac{\partial^2 \psi}{\partial h^2} \approx \frac{\gamma}{(\alpha - \gamma)^2}$, which yields

$$\frac{dK_0(\mathbf{s}(t))}{dt} \approx \left(\alpha + \gamma - \frac{\gamma}{(\gamma - \alpha)^2} \right) K_0(\mathbf{s}(t)). \tag{30}$$

Using (22) we obtain

$$K_0 \sim \left(\frac{x_0}{x_0 + \gamma x} \right)^{\frac{\alpha + \gamma}{\gamma} - \frac{1}{(\alpha - \gamma)^2}}. \tag{31}$$

Finally, for $\mathbf{s} \in V_A$

$$p(\mathbf{s}) \sim K_0(\mathbf{s}) e^{-\frac{\psi(\mathbf{s})}{\sigma}}, \tag{32}$$

where K_0 and ψ are defined by relations (31) and (29), respectively. When $\alpha \neq \gamma$ and $\alpha \neq 2\gamma$, the exponent in (31) is positive when

$$\frac{\alpha + \gamma}{\gamma} - \frac{1}{(\gamma - \alpha)^2} > 0 \iff 1 - \left(\frac{\gamma}{\alpha} \right) - \left(\frac{\gamma}{\alpha} \right)^2 + \left(\frac{\gamma}{\alpha} \right)^3 - \frac{\gamma}{\alpha^3} > 0, \tag{33}$$

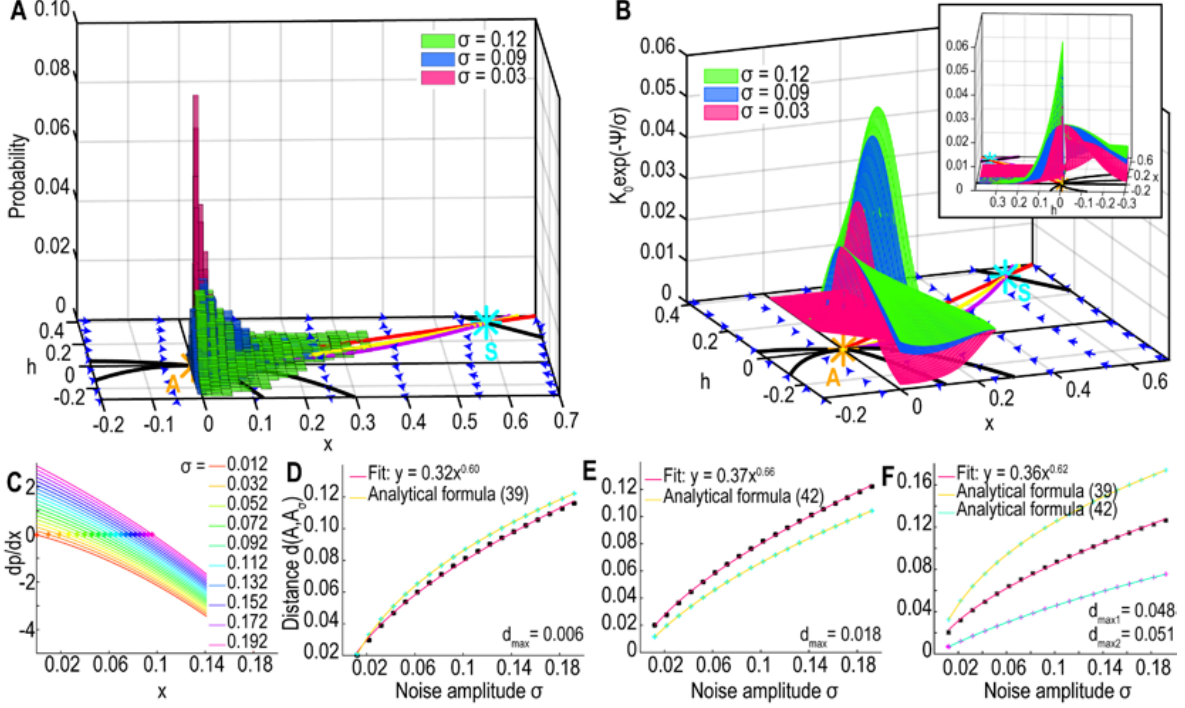


Figure 2: **Position of the shifted attractor A_σ** **A.** Simulated pdf of the trajectories for three noise levels $\sigma = 0.03$ (pink), $\sigma = 0.09$ (blue) and $\sigma = 0.12$ (green) for $\gamma = 0.6$ and $\alpha = 1$. **B.** Analytical distributions for the three noise levels. Inset: same distributions with a different perspective. **C.** $\frac{\partial p}{\partial x}|_{h=0^+}(x)$ for $\sigma \in [0.01, 0.2]$ (the crosses indicate the zeros). **D-E.** Distance $d(A, A_\sigma)$ as a function of σ . Numerical solution (black stars with numerical fit in pink) and analytical relation 39 (resp. 42, cyan crosses with yellow curve) for $\gamma = 0.6$ (resp. 0.9) and $\alpha = 1$. **F.** Distance $d(A, A_\sigma)$ as a function of σ . Numerical solution (black stars with numerical fit in pink) compared with the analytical expressions (39) and (42) (cyan crosses with yellow curve and magenta crosses with blue curve) in the case $\gamma = 0.75$ and $\alpha = 1$ for which neither polynomial approximation is valid.

that is for $\frac{\gamma}{\alpha} > 0.45$. For the range of parameters $0.45\alpha < \gamma < \alpha$ and $\alpha \neq 2\gamma$, the pdf has a maximum located on the $h = 0^+$ axis towards the right of A as shown in fig. 2B for three values of the noise amplitude $\sigma = 0.03$ (pink), 0.09 (blue) and 0.12 green and for $\gamma = 0.6$. This maximum gives the position of the shifted attractor A_σ , which depends on the noise amplitude.

In the case where $\frac{\gamma}{\alpha} \leq 0.45$, since the linearization approximation done in (28) is not anymore valid, we cannot use formula (32) to represent the pdf.

2.2.4 Computing the distance between A_σ and A

In this subsection, we study the distance between A and A_σ with respect to the noise amplitude σ . The maximum of the pdf (32) is given by

$$\nabla p = 0. \quad (34)$$

However, the partial derivative along h is discontinuous, and we observe that the analytical expression for pdf p (24, 32) is decreasing as $|h|$ increases on both halves of the phase-space. Furthermore, numerical simulations show that the maximum of the pdf A_σ is shifted along the x axis. Thus we only need to solve $\frac{\partial p}{\partial x}|_{h=0^+} = 0$. Using relation 32, for $h \geq 0$ we obtain

$$\begin{aligned} -\frac{\left(\frac{\alpha + \gamma}{\gamma} - \frac{1}{(\alpha - \gamma)^2}\right)\gamma}{x_0 + \gamma x} + \frac{1}{\sigma} \left(-\frac{Q_0^2}{q_{2,0}} \left(\frac{2\gamma}{q_{2,0}}\right)^{\frac{2\alpha}{\gamma} - 1} \frac{2\alpha}{x\gamma} - 1 \right. \\ \left. - \frac{2Q_0}{\gamma - \alpha} \left(\frac{2\gamma}{q_{2,0}}\right)^{\frac{\alpha}{\gamma}} \frac{\alpha}{x\gamma} - \frac{2\gamma x}{(\alpha - \gamma)^2} \right) = 0, \end{aligned} \quad (35)$$

We rewrite (35) as

$$-\frac{A_1}{1 + \frac{\gamma}{x_0}x} - \frac{1}{\sigma} \left(A_2 x^{\frac{2\alpha}{\gamma} - 1} + A_3 x^{\frac{\alpha}{\gamma}} + A_4 x \right) = 0, \quad (36)$$

where

$$A_1 = \left(\frac{\alpha + \gamma}{\gamma} - \frac{1}{(\alpha - \gamma)^2}\right) \frac{\gamma}{x_0}, A_2 = \frac{Q_0^2}{q_{2,0}} \left(\frac{2\gamma}{q_{2,0}}\right)^{\frac{2\alpha}{\gamma} - 1}, A_3 = \frac{2Q_0}{\gamma - \alpha} \left(\frac{2\gamma}{q_{2,0}}\right)^{\frac{\alpha}{\gamma}}, A_4 = \frac{2\gamma}{(\alpha - \gamma)^2}. \quad (37)$$

In general, this algebraic equation cannot be solved analytically, we solved it numerically for various values of σ (fig. 2C). We shall now describe two cases for which equation (36) can be approximated by a polynomial equation. We choose the approximation ranges $0.5 < \frac{\gamma}{\alpha} \leq$

0.645 and $0.885 \leq \frac{\gamma}{\alpha} < 1$ by computing the absolute difference $d(\sigma) = |x_{M,num}(\sigma) - x_M(\sigma)|$ between the numerical result $x_{M,num}(\sigma)$ and the solution of the approximated polynomial equation $x_M(\sigma)$ that we define below (equations 39 and 42) for $\sigma \in [0, 0.2]$ and by using the following criteria $d_{max} = \max_{\sigma \in [0, 0.2]} (d(\sigma)) < 0.02$ (fig. 2D-F).

2.2.5 Analytical expression of the distance between A_σ and A in the range $0.5 < \frac{\gamma}{\alpha} < 0.645$

In that range, we approximate $\frac{2\alpha}{\gamma} - 1 \approx 2$ and $\frac{\alpha}{\gamma} \approx 2$ and (36) becomes the third order polynomial equation

$$A_1\sigma + A_4x + \left(A_2 + A_3 + \frac{A_4\gamma}{x_0}\right)x^2 + (A_2 + A_3)\frac{\gamma}{x_0}x^3 = 0. \quad (38)$$

The solution is (fig. 2D, cyan crosses and yellow curve)

$$x_M(\sigma) = \left(\frac{-q(\sigma) - \sqrt{\Delta(\sigma)}}{2}\right)^{1/3} + \left(\frac{-q(\sigma) + \sqrt{\Delta(\sigma)}}{2}\right)^{1/3} - \frac{c_2}{3c_1}, \quad (39)$$

where

$$\begin{aligned} c_1 &= A_2 + A_3 + \frac{A_4\gamma}{x_0} \approx 397, 2 \\ c_2 &= A_2 + A_3 \approx 117.5 \\ A_4 &= 7.5 \\ A_1 &\approx -17.7 \\ q(\sigma) &= \frac{2c_2^3 - 9c_1c_2A_4}{27c_1^3} + \frac{A_1}{c_1}\sigma \approx 5, 5 \cdot 10^{-5} - 0.04\sigma \\ \Delta(\sigma) &= q(\sigma)^2 + \frac{4}{27} \left(\frac{3c_1A_4 - c_2^2}{3c_1^2}\right)^3 \approx q(\sigma)^2 - 1, 6 \cdot 10^{-7}, \end{aligned} \quad (40)$$

for the parameter values $\alpha = 1, \gamma = 0.6, h_0 = 0.001, x_0 = 0.12$. Expression (39) is valid as long as $\Delta(\sigma) \geq 0$, yielding $\sigma > 0.0114$.

2.2.6 Analytical expression of distance between A_σ and A in the range $0.885 \leq \frac{\gamma}{\alpha} < 1$

In the range $0.9 \leq \frac{\gamma}{\alpha} < 1$ we approximate (36) by the second order polynomial equation

$$\frac{\gamma}{x_0}x^2 + x + \frac{A_1\sigma}{A_2 + A_3 + A_4} = 0, \quad (41)$$

the solution is

$$x_M(\sigma) = \frac{-1 + \sqrt{1 - \frac{4\gamma}{x_0} \frac{A_1\sigma}{A_2 + A_3 + A_4}}}{2\gamma} x_0 \approx -0.56 + \frac{\sqrt{1 + 38.45\sigma}}{1.8}, \quad (42)$$

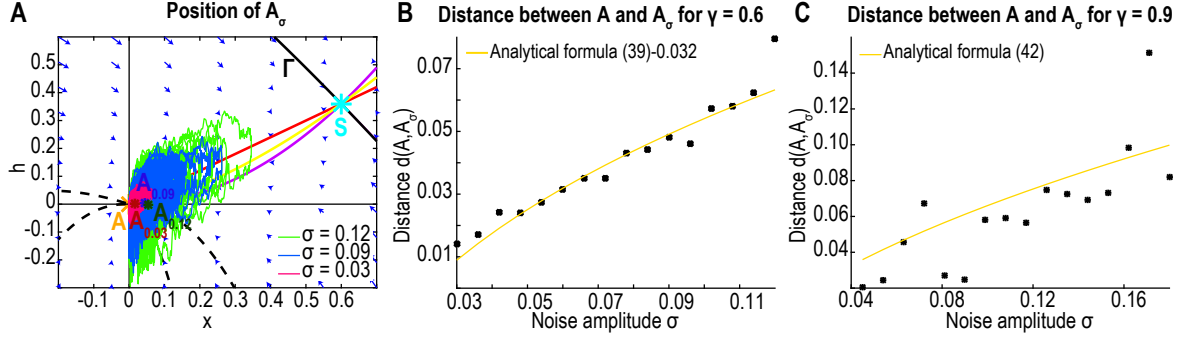


Figure 3: **Influence of the noise amplitude on the position of A_σ .** **A.** Stochastic trajectories simulated for $T = 500s$ for three noise levels $\sigma = 0.03$ (pink), 0.09 (blue) and 0.12 (green) and the shifted attractors A_σ . **B.** $d(A, A_\sigma)$ with respect to σ , numerical simulations ($T = 800s$ per noise value, black stars) compared to the analytical formula 39 (yellow) minus a corrective offset $\hat{c} = 0.032$. **C.** $d(A, A_\sigma)$ with respect to σ , numerical simulations ($T = 800s$ per noise value, black dots) compared to the analytical formula 42 (yellow).

for the parameter values $\alpha = 1$, $\gamma = 0.9$ and $\sigma \geq 0$ (fig. 2E cyan crosses and yellow curve). To test the range of validity of our approximations for the position of A_σ , we ran simulations for $\sigma \in [0.03, 0.12]$ (fig. 3A $\sigma = 0.12$, green, 0.09 , blue and 0.03 , pink). We compared the distance $d(A, A_\sigma)$ obtained from numerical simulations (3B-C black stars) and the analytical formula (39) (resp. 42) (fig. 3B (resp. C) yellow curve) for $\alpha = 1$ and $\gamma = 0.6$ (resp. $\gamma = 0.9$). In the case $\gamma = 0.6$, we added an offset in formula (39) to minimize the absolute value of the difference between the analytical formula and the simulations:

$$\hat{c} = \min_{c \in [0, 0.1]} \sum_{\sigma \in [0.03, 0.12]} |x_M(\sigma) - c - x_{M, sim}(\sigma)|, \quad (43)$$

where $x_M(\sigma)$ is defined by (39) and $x_{M, sim}(\sigma)$ is the value obtained from the numerical simulations. Using a finite number of values we directly found that $\hat{c} = 0.032$. This offset is probably due to the approximations we made for the derivation of formula (39). To conclude we have found here analytical expressions (39 and 42) for the position of A_σ and shown that these expressions approximate well the numerical simulations.

3 Distributions of escape times and points

3.1 The different phases of the escape process

The escape process can be divided into three steps. Step 1: starting from the attractor A , trajectories fall into the basin of attraction of the shifted equilibrium A_σ . The duration of this step is almost immediate and can be neglected compared with the durations of steps 2 and 3. Step 2: trajectories fluctuate around the shifted equilibrium A_σ until they reach the separatrix Γ for the first time. Step 3: trajectories cross Γ , exiting and reentering the basin

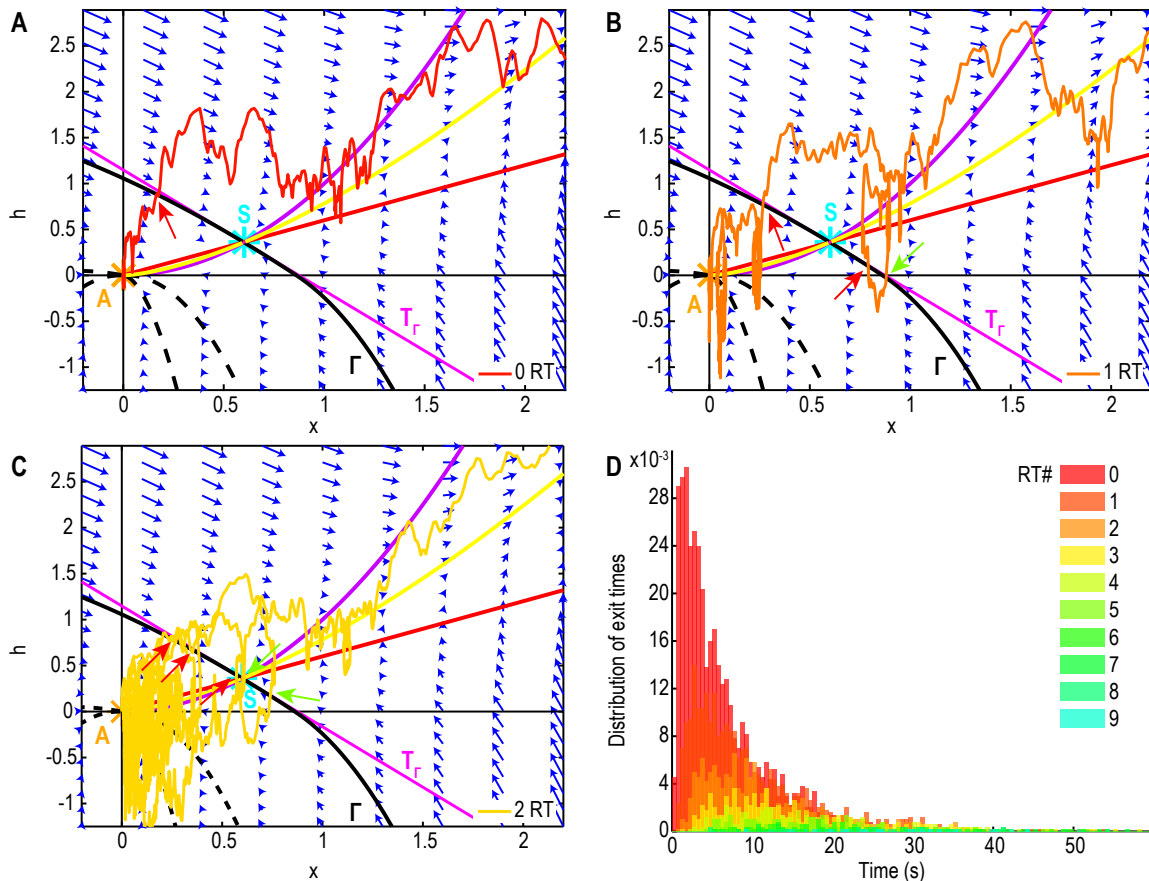


Figure 4: **Recurrent exit pattern and contribution to the escape time.** **A-C.** Trajectory doing zero (resp. one, two) RT before escape (red, resp. orange, yellow) the red (resp. green) arrows indicate exit (resp. reentry) points. **D.** Distribution of escape times from 5000 trajectories lasting $T=300s$ ($\gamma = 0.6$, $\alpha = 1$ and $\sigma = 0.78$) with the contribution of trajectories doing for each number of RT around Γ before escaping (color gradient).

of attraction several times before eventually escaping far away (fig. 4A-C). We quantified these excursions by counting the number of round-trips (RT) across Γ .

We studied these three steps numerically by simulating 5000 trajectories starting from A and lasting $T = 300s$ for $\sigma = 0.78$. To study the distribution of exit times and points on the separatrix Γ at each RT we decided to replace Γ by its tangent T_Γ at S (fig. 4A-C pink line), indeed, the distribution of exit points peaks at a distance $O(\sqrt{\sigma})$ from S [20] and thus the difference between the separatrix and its tangent is of order 2. That will allow us to use the analytical expression of the tangent T_Γ .

We could thus decompose the escape time in the time to reach Γ for the first time plus the time spent doing successive excursions outside and inside the basin of attraction (fig. 4D, the gradient of colors indicates the contribution of the trajectories doing a specific number of RT to the total distribution of escape times). Finally, we could estimate the proportion of trajectories that escape at each RT to evaluate the probability to escape after crossing the separatrix as we will detail below.

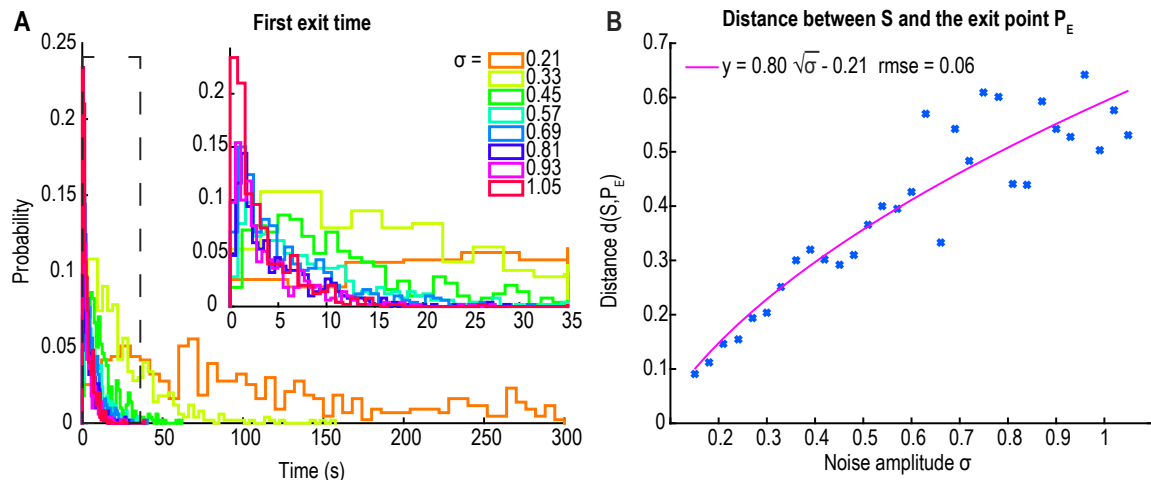


Figure 5: **Influence of the noise amplitude on the first exit times and points.** **A.** Distribution of the first exit times with respect to the noise amplitude σ with an inset on short times. **B.** Distance between the peak P_E of the distribution of first exit points on the separatrix and the saddle-point S with respect to the noise amplitude σ for $\gamma = 0.6$ and $\alpha = 1$ with a square-root fit (magenta).

3.2 Distributions of the first exit times and exit points on the separatrix

We studied the influence of the noise on the distributions of first exit times and exit points: we simulated $N = 2500$ trajectories starting at A and lasting $T = 300s$ for $\sigma \in [0.21, 1.05]$. The first exit time can be very long for small values of σ (fig. 5A, orange distribution for $\sigma = 0.21$, and light green for $\sigma = 0.33$) but becomes shorter with peaked distributions when σ increases (dark green to red). The distribution of the first exit points is peaked and located on the left of the saddle-point S (fig. A.1A purple for $\sigma = 0.78$). We found here that the distance $d(P_E, S)$ between the peak P_E of this distribution and the saddle-point S for $\sigma \in [0.15, 1.05]$ is of order $O(\sqrt{\sigma})$ (fig. 5B) in agreement with the classical theory [20]. We further observed from numerical simulations that the first exit points of trajectories that reenter the basin of attraction at least once follow a similar distribution as the one of first exit points for all trajectories (fig. A.1A green) indicating that there are no correlations between the position of the escape point and the phenomenon of reentry in the basin of attraction. Finally, the distribution of the first reentry points also peaks on the left of the saddle-point but spreads on both sides of S (fig. A.1A red).

3.3 Characterization of the mean escape time

To compute the mean escape time, we use Baye's law and condition by the RT numbers so that

$$\langle \tau_{esc} \rangle = \sum_{k=0}^{\infty} \langle \tau | k \rangle P_{RT}(k), \quad (44)$$

where $\langle \tau|k \rangle$ (resp. $P_{RT}(k)$) is the mean time (resp. probability) to return k times inside the basin of attraction. Because the RT are independent events, the probability \tilde{p} that a trajectory crossing the separatrix Γ escapes does not depend on k , yielding

$$P_{RT}(k) = \tilde{p}(1 - \tilde{p})^{k-1}, \quad (45)$$

thus

$$\langle \tau_{esc} \rangle = \langle \tau_0 \rangle + (\langle \tau_{ext} \rangle + \langle \tau_{int} \rangle) \tilde{p} \sum_{k=1}^{\infty} k(1 - \tilde{p})^{k-1} = \langle \tau_0 \rangle + \frac{\langle \tau_{ext} \rangle + \langle \tau_{int} \rangle}{\tilde{p}}, \quad (46)$$

where $\langle \tau_{ext} \rangle$ (resp. $\langle \tau_{int} \rangle$) is the mean time spent outside (resp. inside) the basin of attraction during one RT. To avoid counting small Brownian fluctuations as RT (fig. 6A black arrows), we added a second line $\tilde{\Gamma}$ at distance $\delta = 0.25$ from the separatrix (fig. 6B blue line) and thus a trajectory is considered to have exited the basin of attraction once it has crossed both the tangent T_Γ and $\tilde{\Gamma}$.

Using this procedure we estimated the probability $\tilde{p}(k)$ to escape after k RT by counting the proportion of trajectories that reenter the basin of attraction at least once and we found using numerical simulations $\tilde{p}(1) \approx 0.40$. We iterated this process for each RT until all the trajectories had escaped to infinity and found that $\tilde{p}(k)$ for $k \geq 1$ does not depend on k (fig. A.1B), thus $\tau_{esc} \approx \tau_0 + 2.5(\tau_{ext} + \tau_{int})$. Finally, with the parameters $\alpha = 1$, $\gamma = 0.6$ and $\sigma = 0.78$, numerical simulations show that $\langle \tau_0 \rangle \approx 5s$ and $\langle \tau_{ext} \rangle + \langle \tau_{int} \rangle \approx 2.6s$ (fig. 6C). To conclude, the process of entering and exiting multiple times increases the mean escape time by a factor of 2.3. In addition we found, based on simulations for $\sigma \in [0.54, 0.90]$, that the noise amplitude does not influence the number of RT before escape (fig. 6D) and that trajectories perform 2.5 RT on average.

3.4 Characterization of escape times distributions

To determine the distribution of escape times, we condition on the number of RT, so that

$$P(\tau_{esc} < t) = \sum_{k=0}^{\infty} P(\tau^k < t|k)P_{RT}(k), \quad (47)$$

where $P(\tau^k < t|k)$ is the probability distribution of escape times after k RT. This probability is obtained by the k -th convolution of the distribution f_1 of times for trajectories exiting after a single RT with the distribution f_0 of escape times with 0 RT

$$P(\tau^k < t|k) = f_0(t) * f_1(t)^{*k}, \quad (48)$$

where $f(t)^{*k} = f(t) * f(t) * \dots * f(t)$, k times. Thus (47) becomes

$$P(\tau_{esc} < t) = \sum_{k=0}^{\infty} f_0(t) * f_1(t)^{*k} \tilde{p}(1 - \tilde{p})^k. \quad (49)$$

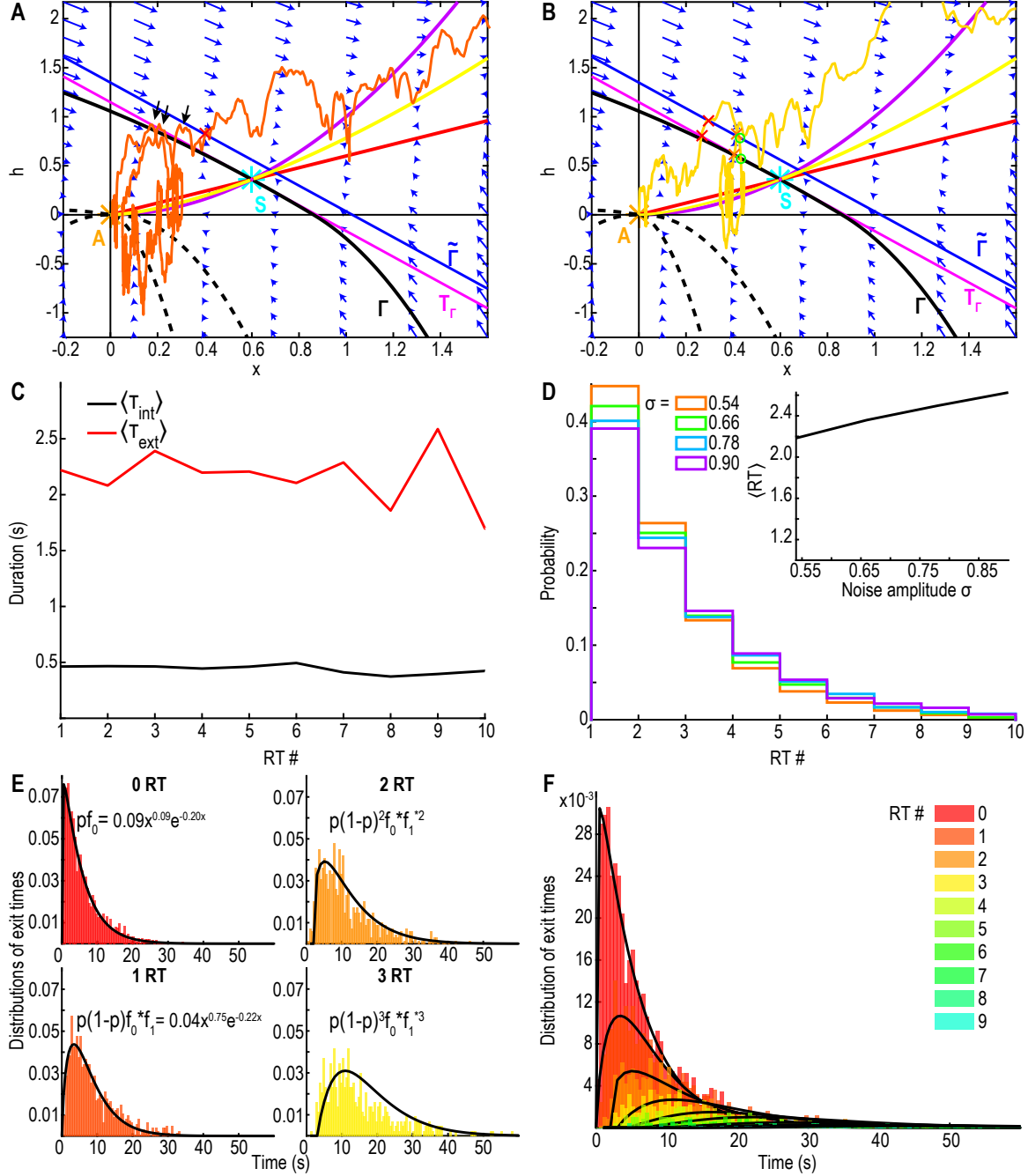


Figure 6: **Characterization of escape times.** **A.** Trajectory escaping (red cross) after small brownian fluctuations at the separatrix (black arrows). **B.** Trajectory exiting (red crosses) after crossing T_Γ (pink) and $\tilde{\Gamma}$ (blue), reentering (green circles) and reexiting (orange crosses) the basin of attraction before escaping. **C.** Mean time $\langle \tau_{ext} \rangle$ (resp. $\langle \tau_{int} \rangle$) spent outside (resp. inside) the basin of attraction at each RT. **D.** Distributions of the RT number before trajectories escape to infinity for $\sigma \in [0.54, 0.90]$. Inset: mean RT number $\langle RT \rangle$ with respect to the noise amplitude. **E.** Distribution of exit times for trajectories doing 0 (upper left, resp. 1 (lower left), 2 (upper right), 3 (lower right)) RT before escape. **F.** Distribution of exit times with the contribution of each RT number (color gradient) with the analytical distribution (49) (black)

To compare this formula with our numerical results, we decided to fit the distributions with

$$f_i(t) = c_i t^{a_i} e^{-\lambda_i t}, \text{ for } i = 0, 1, a_i \geq 0 \text{ and } \lambda_i \geq 0 \quad (50)$$

We obtained, using the Matlab fit function (fig. 6C) for the distribution of trajectories that escape without doing any RT

$$\tilde{p}f_0(t) = 0.09t^{0.09}e^{-0.20t} \quad (51)$$

and for the trajectories doing exactly one RT before escape

$$F_1(t) = \tilde{p}(1 - \tilde{p})f_0 * f_1(t) = 0.04t^{0.75}e^{-0.22t}. \quad (52)$$

To recover the distribution f_1 (52) we deconvolved numerically F_1 from f_0 (51) (fig. 6E lower left). This procedure allows us to validate our approach by computing the distributions of 2 and 3 RT and comparing them with the empirical distributions (48) (fig. 6E upper and lower right). Finally, we decomposed the entire escape times distribution using (49) to evaluate the contribution of each term (fig. 6E-F).

4 Application to interburst durations in neuronal networks

We shall now present an application in computational neuroscience of the results presented in the sections above. Neuronal networks can be modeled in the mean-field approximation by stochastic differential equations. In particular it is possible to study bursting dynamics accounting for short-term synaptic plasticity (depression and facilitation) [10, 14, 15]. We propose here to study the distribution of interburst intervals that exactly represents the escape from a basin of attraction with similar properties as presented in equation (1). We shall use here a version of the depression-facilitation model which consists in three coupled equations for the mean voltage h , the depression y , and the synaptic facilitation x :

$$\begin{aligned} \tau \dot{h} &= -h + Jxyh^+ + \sqrt{\tau}\sigma\dot{\omega} \\ \dot{x} &= \frac{X-x}{t_f} + K(1-x)h^+ \\ \dot{y} &= \frac{1-y}{t_r} - Lxyh^+, \end{aligned} \quad (53)$$

where the population average firing rate $h^+ = \max(h, 0)$ is a linear threshold function of the synaptic current. The mean number of connections (synapses) per neuron is accounted for by the parameter J and the term Jxy reflects the combined effect of the short-term synaptic plasticity on the network's activity. We previously distinguished [15] the parameters K and L which describe how the firing rate is transformed into molecular events that are changing the duration and probability of vesicular release. The time scales t_f and t_r define the recovery of a synapse from the network activity. Finally, $\dot{\omega}$ is an additive Gaussian noise and σ its

amplitude. System (53) has 3 critical points: one attractor and two saddle-points. At the attractor $A = (0, X, 1)$, the dynamics is very anisotropic

$$\left(|\lambda_1| = \frac{1 - JX}{\tau} \approx 12.6 \gg |\lambda_2| = \frac{1}{\tau_f} \approx 1.1 \gg |\lambda_3| \approx \frac{1}{\tau_r} = 0.34, \text{ using parameters in table 4} \right)$$

and can thus be reduced to a 2D-plan $y = Cte$ so that

$$\dot{y} = 0 = \frac{1 - y}{\tau_r} - Lxyh^+ = 0 \iff y = \frac{1}{1 + \tau_r Lxh^+}, \quad (54)$$

and we obtain

$$\begin{aligned} \dot{h} &= \frac{h(Jx - 1 - \tau_r Lxh^+)}{\tau(1 + \tau_r Lxh^+)} + \sqrt{\tau}\sigma\dot{\omega} \\ \dot{x} &= \frac{X - x}{\tau_f} + K(1 - x)h^+. \end{aligned} \quad (55)$$

The deterministic system (55) (for $\sigma = 0$) has 3 critical points, two attractors and one saddle-point:

Attractor A_0 is given by $h = 0$ and $x = X$. The Jacobian is

$$J_{A_0} = \begin{pmatrix} \frac{-1 + JX}{\tau} & 0 \\ K(1 - X) & -\frac{1}{\tau_f} \end{pmatrix}. \quad (56)$$

With our parameters (table 4) the eigenvalues are $(\lambda_1, \lambda_2) = \left(\frac{JX - 1}{\tau}, \frac{1}{\tau_f} \right) \approx (-12.6, -1.11)$.

Saddle-point S is $S_1(h_1 \approx 8.07; x_1 \approx 0.28)$. Its eigenvalues are $(\lambda_1, \lambda_2) \approx (-5.73, 1.43)$ and $\lambda_2 \approx 1.43$.

Attractor A_2 is $A_2(h_2 \approx 28.8; x_2 \approx 0.53)$. Its eigenvalues are $(\lambda_1, \lambda_2) \approx (-11.9, -1.33)$. The two attractors are separated by the 1D stable manifold of the saddle-point S (fig. 7A, solid black curve). The phase-space, restricted to $\{x \leq 0.5 \text{ and } h \leq 30\}$ is topologically equivalent to the phase-space of system (1). It has one attractor and one saddle-point and the stable manifold of the saddle-point defines the boundary of the basin of attraction (fig. 7A). Similar to system (1) the trajectories fall into a basin of attraction centered around a shifted attractor towards the saddle-point S (fig. 7B, red (resp. blue, green) star for $\sigma = 1$ (resp. 1.5, 2.5)), the shift in the attractor's position depends on the noise amplitude (fig. 7C) and the escaping trajectories can return several times inside the basin of attraction before

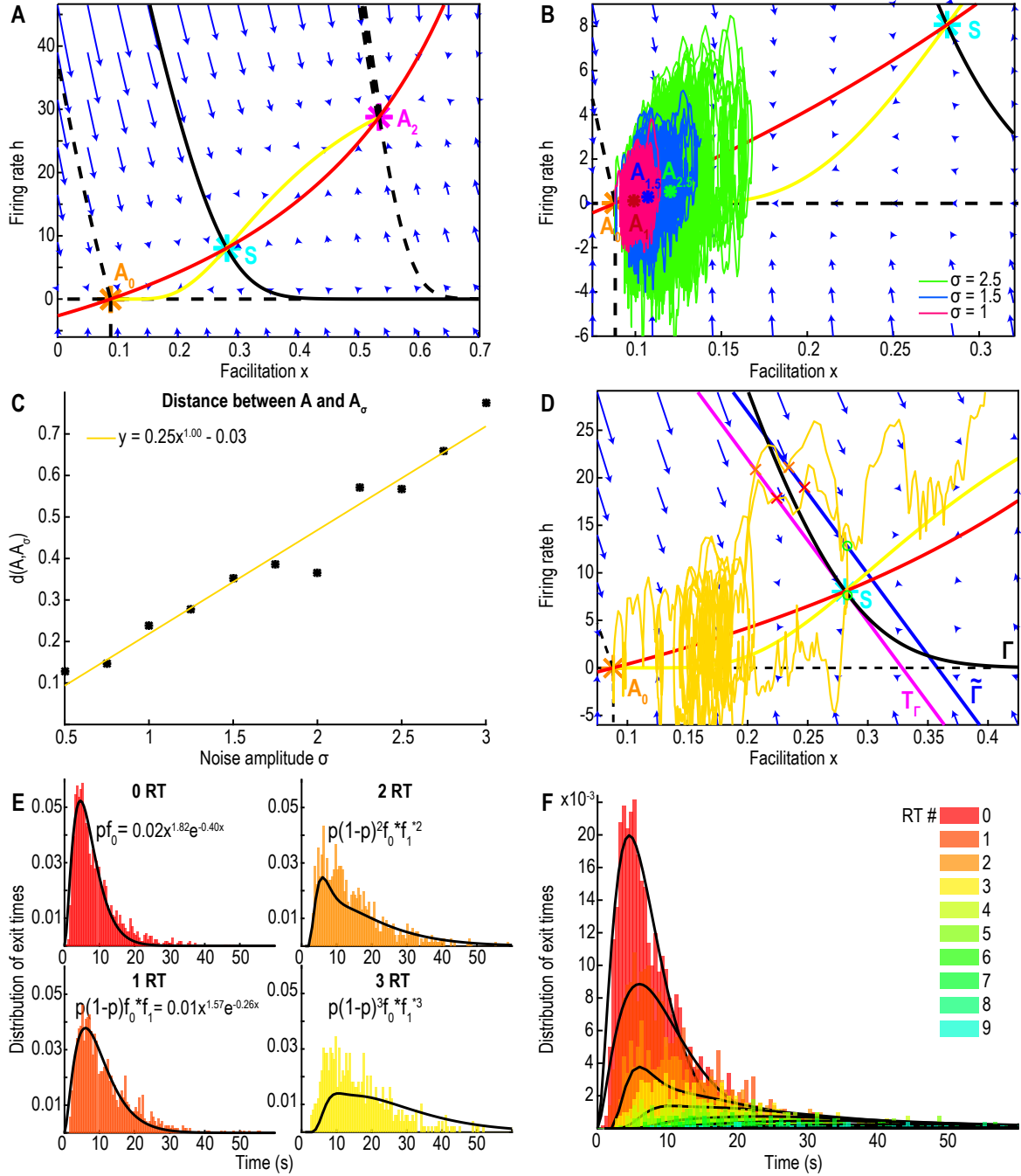


Figure 7: **Application to the facilitation-depression model** (53). **A.** Phase-space of system (55), attractors A_0 (yellow) and A_2 (pink) and saddle-point S (cyan). The stable manifold of S (solid black) separates the two basins of attraction. **B.** Inset near A_0 and S with trajectories ($T = 500s$) for three noise levels $\sigma = 1$ (pink), 1.5 (blue) and 2.5 (green) and shifted attractors A_σ . **C.** Distance $d(A_0, A_\sigma)$ for $\sigma \in [0.5, 3]$ with a numerical fit (yellow). **D.** Trajectory doing 1 RT before escape. **E.** Distribution of exit times for trajectories doing 0 (upper left, resp. 1 (lower left), 2 (upper right), 3 (lower right)) RT before escape. **F.** Distribution of exit times with the contribution of each RT number (color gradient) with the analytical distribution (49) (black).

escaping far away (fig. 7D, one RT). We used formula (49) to fit the distribution of exit times (fig. 7E-F). We obtained, for $\sigma = 6$

$$f_0(t) = 0.02t^{1.82}e^{-0.40t} \quad (57)$$

and

$$f_1(t) = 0.01t^{1.57}e^{-0.26t}. \quad (58)$$

Finally, our numerical simulations give $\tilde{p} \approx 0.37$ (fig. A.2A) and the mean escape time is given by formula (46): $\langle \tau_{esc} \rangle \approx \langle \tau_0 \rangle + 2.7(\langle \tau_{ext} \rangle + \langle \tau_{int} \rangle)$. With the parameters of table 4, we obtain $\langle \tau_0 \rangle \approx 4.35s$ and $\langle \tau_{ext} \rangle + \langle \tau_{int} \rangle \approx 2.6s$ (fig. A.2B) thus increasing the escape time by a factor 2.6. As seen in section 3.3 The number of RT done before escape does not depend on the noise amplitude (fig. A.2C) and the trajectories do on average 2.7 RT before escape (fig. A.2C, inset). To conclude, this escape mechanism could explain long interburst durations that can occur in excitatory neuronal networks without the need of adding a refractory mechanism.

Conclusion

We studied here a class of stochastic dynamical systems perturbed by a small Gaussian noise. The main findings are a pdf that peaks at a maximum which is not the attractor and a non classical escape characterized by multiple reentries inside the attractor. We computed the position of this shifted attractor using WKB approximation and we derived algebraic formulas to link the position to the noise amplitude σ (formulas 39 and 42). We also computed the escape time that we decomposed into the time to reach the boundary of the basin of attraction plus the time spent going back and forth through the separatrix (formulas 46 and 49).

Finally, we applied our computations to describe and to quantify neuronal bursting dynamics modeled in the mean-field approximation by depression-facilitation equations [10, 15]. We thus provided an elementary explanation for the long interburst durations observed in neuronal networks [16].

Acknowledgement

L. Zonca has received support from the FRM (FDT202012010690). This work was funded by This project has received funding from the European Research Council (ERC) under the European Union’s Horizon 2020 research and innovation programme (grant agreement No 882673).

Appendix

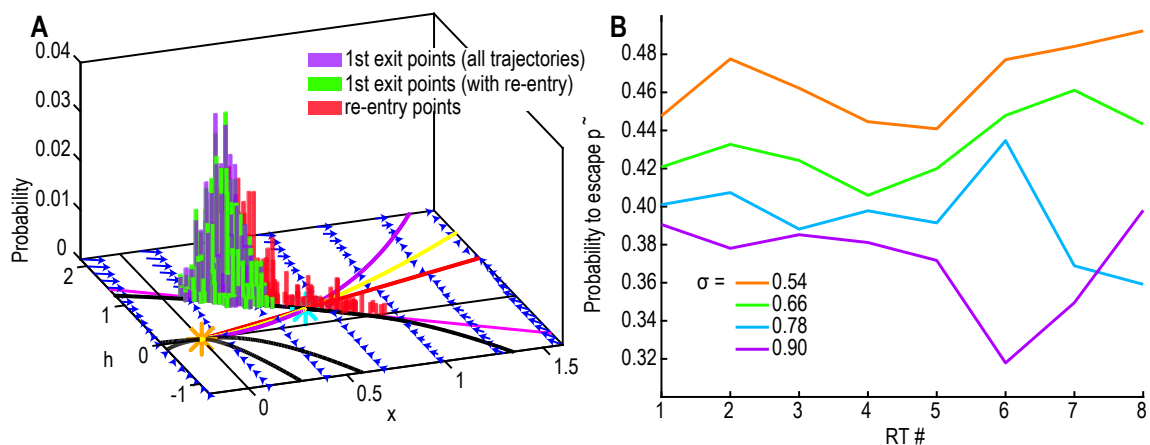


Figure A.1: **A.** Distributions of the first exit points on Γ (purple), the first exit points of the trajectories that reenter the basin of attraction at least once (green, 60% of trajectories), the points where these trajectories reenter the basin of attraction for the first time (red) for $\sigma = 0.78$. **B.** Probability to escape after exiting the basin of attraction for the k -th time, $\tilde{p}(k)$ estimated by the proportion of trajectories that reenter the basin of attraction after k RT for noise amplitudes $\sigma \in [0.54, 0.90]$.

	Parameters	Values
τ	Time constant for h	0.05s
J	Synaptic connectivity	4.21
K	Facilitation rate	0.037Hz
X	Facilitation resting value	0.08825
L	Depression rate	0.028Hz
τ_r	Depression time rate	2.9s
τ_f	Facilitation time rate	0.9s
T	Depolarization parameter	0

References

- [1] M. I. Dykman, M. M. Millonas, and V. N. Smelyanskiy, “Observable and hidden singular features of large fluctuations in nonequilibrium systems,” *Physics Letters A*, vol. 195, no. 1, pp. 53–58, 1994.
- [2] M. I. Dykman, E. Mori, J. Ross, and P. Hunt, “Large fluctuations and optimal paths in chemical kinetics,” *The Journal of chemical physics*, vol. 100, no. 8, pp. 5735–5750, 1994.

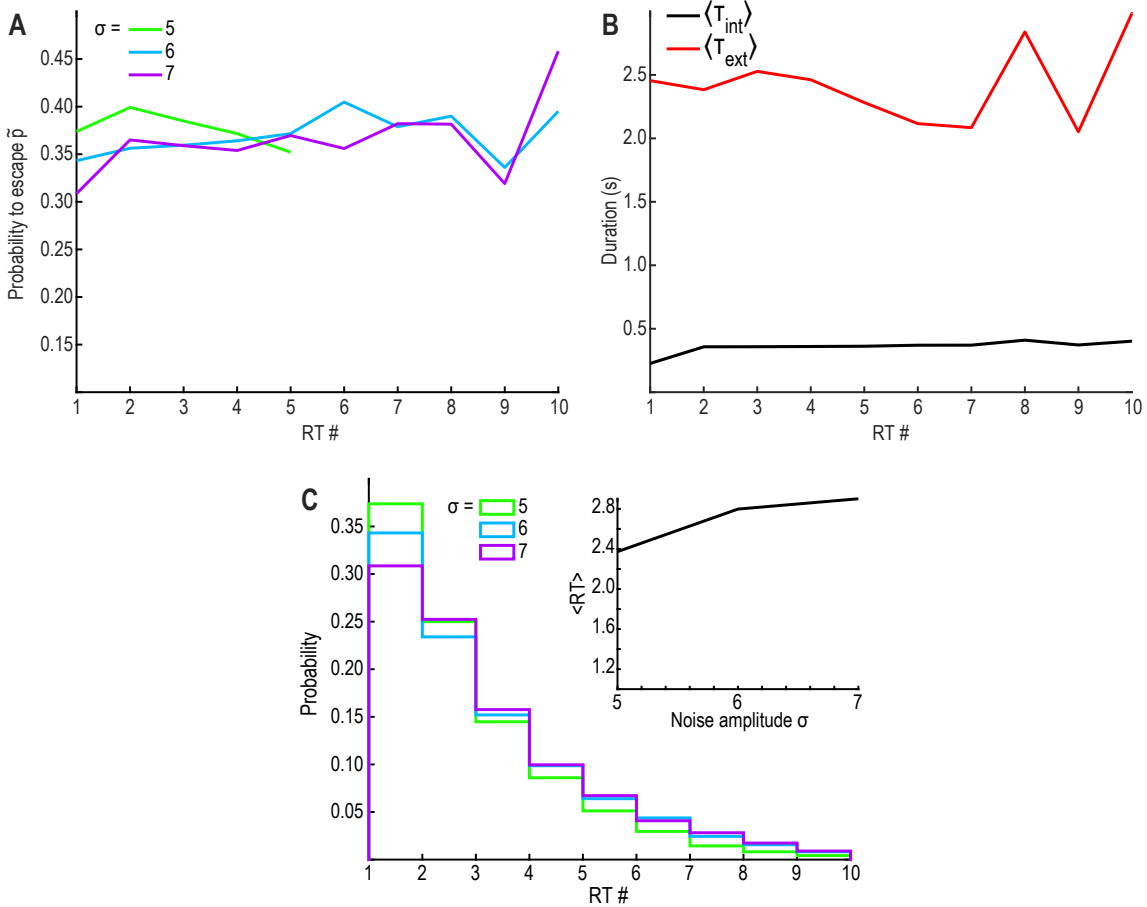


Figure A.2: **A.** Probability \tilde{p} to escape after exiting the basin of attraction with respect to the RT number for $\sigma \in [4, 7]$, with a linear fit. **B.** Values of $\langle T_{ext} \rangle$ (red) and $\langle T_{int} \rangle$ (black) with respect to the RT number. **C.** Distributions of the RT number before escape for $\sigma \in [4, 7]$. Inset: mean RT number with respect to σ

- [3] R. S. Maier and D. L. Stein, “Effect of focusing and caustics on exit phenomena in systems lacking detailed balance,” *Phys. Rev. Lett.*, vol. 71, pp. 1783–1786, Sep 1993.
- [4] B. Lindner, J. García-Ojalvo, A. Neiman, and L. Schimansky-Geier, “Effects of noise in excitable systems,” *Physics reports*, vol. 392, no. 6, pp. 321–424, 2004.
- [5] R. Kuske, “Multi-scale analysis of noise-sensitivity near a bifurcation,” in *Nonlinear stochastic dynamics* (N. Namachchivaya and Y. Lin, eds.), pp. 147–156, Springer Science+Business Media Dordrecht, 2003.
- [6] L. Schimansky-Geier, A. Tolstopjatenko, and W. Ebelin, “Noise induced transitions due to external additive noise,” *Physics Letters A*, vol. 108, no. 7, pp. 329–332, 1985.
- [7] L. Arnold, “A new example of an unstable system being stabilized by random parameter noise,” *Inform. Comm. Math. Chem*, vol. 7, pp. 133–140, 1979.

- [8] L. Arnold, “Stabilization by noise revisited,” *ZAMM-Journal of Applied Mathematics and Mechanics/Zeitschrift für Angewandte Mathematik und Mechanik*, vol. 70, no. 7, pp. 235–246, 1990.
- [9] V. Wihstutz, “On stabilizing the double oscillator by mean zero noise,” in *Nonlinear stochastic dynamics* (N. Namachchivaya and Y. Lin, eds.), pp. 179–190, Springer Science+Business Media Dordrecht, 2003.
- [10] M. V. Tsodyks and H. Markram, “The neural code between neocortical pyramidal neurons depends on neurotransmitter release probability,” *Proc. Natl. Acad. Sci. USA*, vol. 94, pp. 719–723, January 1997.
- [11] N. Brunel and V. Hakim, “Fast global oscillations in networks of integrate-and-fire neurons with low firing rates,” *Neural Computation*, vol. 11, pp. 1621–1671, November 1999.
- [12] L. Neltner and D. Hansel, “On synchrony of weakly coupled neurons at low firing rate,” *Neural Computation*, vol. 13, pp. 765–774, April 2001.
- [13] D. Holcman and M. Tsodyks, “The emergence of up and down states in cortical networks,” *PLoS Computational Biology*, vol. 2, pp. 174–181, March 2006.
- [14] O. Barak and M. Tsodyks, “Persistent activity in neural networks with dynamic synapses,” *PLoS Computational Biology*, vol. 3, no. 2, 2007.
- [15] K. Dao Duc, C.-Y. Lee, P. Parutto, D. Cohen, M. Segal, N. Rouach, and D. Holcman, “Bursting reverberation as a multiscale neuronal network process driven by synaptic depression-facilitation,” *Plos one*, vol. 10, no. 5, p. e0124694, 2015.
- [16] O. Chever, E. Dossi, U. Pannasch, M. Derangeon, and N. Rouach, “Astroglial networks promote neuronal coordination,” *Science signaling*, vol. 9, January 2016.
- [17] B. J. Matkowsky and Z. Schuss, “The exit problem for randomly perturbed dynamical systems,” *SIAM Journal on Applied Mathematics*, vol. 33, no. 2, pp. 365–382, 1977.
- [18] Z. Schuss, *Diffusion and Stochastic Processes. An Analytical Approach*. Springer-Verlag, New York, NY, 2009.
- [19] Z. Schuss, *Theory and Applications of Stochastic Differential Equations*. Wiley, 1980.
- [20] B. Bobrovsky and Z. Schuss, “A singular perturbation method for the computation of the mean first passage time in a nonlinear filter,” *SIAM Journal on Applied Mathematics*, vol. 42, no. 1, pp. 174–187, 1982.
- [21] R. S. Maier and D. L. Stein, “Oscillatory behavior of the rate of escape through an unstable limit cycle,” *Phys. Rev. Lett.*, vol. 77, pp. 4860–4863, Dec 1996.
- [22] T. Verechtchaguina, I. M. Sokolov, and L. Schimansky-Geier, “First passage time densities in resonate-and-fire models,” *Physical Review E*, vol. 73, no. 3, p. 031108, 2006.

- [23] T. Verechtchaguina, I. M. Sokolov, and L. Schimansky-Geier, “First passage time densities in non-markovian models with subthreshold oscillations,” *EPL (Europhysics Letters)*, vol. 73, no. 5, p. 691, 2006.
- [24] T. Verechtchaguina, I. M. Sokolov, and L. Schimansky-Geier, “Interspike interval densities of resonate and fire neurons,” *Biosystems*, vol. 89, no. 1-3, pp. 63–68, 2007.
- [25] K. Dao Duc, Z. Schuss, and D. Holcman, “Oscillatory survival probability: Analytical and numerical study of a non-poissonian exit time,” *Multiscale Modeling & Simulation*, vol. 14, no. 2, pp. 772–798, 2016.
- [26] K. Dao Duc, Z. Schuss, and D. Holcman, “Oscillatory decay of the survival probability of activated diffusion across a limit cycle,” *Physical Review E*, vol. 89, no. 3, p. 030101, 2014.
- [27] V. Smelyanskiy, M. Dykman, and B. Golding, “Time oscillations of escape rates in periodically driven systems,” *Physical review letters*, vol. 82, no. 16, p. 3193, 1999.
- [28] M. I. Dykman and D. Ryvkine, “Synchronization of noise-induced escape: how it starts and ends,” in *Noise in Complex Systems and Stochastic Dynamics III*, vol. 5845, pp. 228–237, International Society for Optics and Photonics, 2005.